ingegneria sismica
International Journal of Earthquake Engineering
Anno XLIII - Num. 2 - 2026

Data-physics fusion-based dual-drive dynamic simulation of power system digital twins

Pengfei Jia[1], *Jiayun Zhu*[1,*], *Huiyuan Zhang*[1] *and Yuqiu Lei*[1]

[1] High Voltage Research Institute, China Electric Power Research Institute, Beijing 100192, Beijing, China

SUMMARY: *Digital twin technology, as an important digitization tool, has become a new approach for power system transformation and upgrading. In this paper, a new power system modeling method and framework driven by data-physics fusion is proposed with digital twin technology as the core. Specific research is carried out for the power system frequency response prediction problem, the improved SFR model is used as the physical model, and the two-branch network model (TBNAM) based on attention mechanism is selected as the data-driven model, which realizes the construction of the data-physical fusion model TBNAM-ISFR. The simulation results show that the TBNAM-ISFR model can be effectively applied to the electromechanical transient simulation of the power system driven by the data-physical fusion modeling, and the average absolute errors of the power angle and voltage magnitude under each scenario do not exceed 1.40% and 0.22%, respectively, with good generalization ability to meet the computational requirements of various scenarios. Compared with other comparative models, the TBNAM-ISFR model has the smallest frequency response prediction error value in different power systems, while the prediction time is only 0.21ms, which can simultaneously meet the requirements of accuracy and timeliness in online applications.*

KEYWORDS: *digital twin technology; power system; data-physical fusion drive; SFR; system frequency response; TBNAM model*

1 Introduction

Technological innovations and developments have driven the rapid development of various industries, and modern technological trends including big data, cloud computing, and the Internet of Things are no longer a conceptualized term, but exist in every aspect of our lives [1, 2]. It is also an important product of the development of the digital industrial revolution. Digital twin technology as an emerging technology application will also become a new kind of model to provide direction for the development of power system applications and business upgrading [3, 4].

Under the data-physical fusion, the power system digital twin dual-drive dynamic simulation technology lies in the fusion of IoT data and physical mechanism model through the use of the Internet of Things (IoT), so as to construct a virtual mapping with high fidelity and interactivity, in order to realize the reliability assessment of the power system, operation optimization, automation control, etc. [5-8]. The safe and reliable operation of power system is the foundation of power system development [9]. The digital twin technology can establish a digital twin model of the power system for reliability assessment of the power system [10].

*eprilhkz1215@126.com
https://doi.org/10.65102/is20261034
Published: 30 April, 2026

Reliability assessment includes the failure probability of important equipment, power system load capacity, and power system failure rate [11, 12]. Digital twin technology can help analyze and assess the reliability of the power system, identify the problems of the power system, and improve the operational reliability of the power system [13-15].

In addition, digital twin technology can simulate the operation state of the power system and optimize the operation of the power system by simulating and analyzing the operation parameters of the power system [16, 17]. Power system operation optimization includes load balance, distribution of power electricity, and adjustment of power system parameters [18]. Digital twin technology can help to analyze and optimize the operation parameters of the power system, reduce the operation cost of the power system, and improve the productivity of the power system [19-21]. And in the realization of automation control including online monitoring, automatic scheduling, and automatic alarm [22]. Digital twin technology can be used for power system, digital modeling, monitoring, scheduling, alarming and other operations of the power system through the digital model, to improve the degree of automation of the power system and reduce the cost of operation and maintenance [23-25].

In this paper, a new power system digital twin framework based on data-physical fusion model is constructed, in which the physical model is used as the SFR model and the system frequency response correction model based on the machine learning method is utilized to improve the computational accuracy of the SFR model. The data-driven model used is the two-branch network model based on attention mechanism (TBNAM), which integrates BiLSTM, CNN, and attention mechanism, and is able to process system timing data to extract timing features and correct the SFR prediction results. In order to verify the effectiveness of the proposed data-physics fusion model TBNAM-ISFR in the dynamic analysis of system frequency response, this paper carries out simulation validation and arithmetic case analysis to test the accuracy and generalization ability of the model and compare the prediction results with other models.

2 Digital twin framework for power systems based on data-physical fusion

This chapter takes the digital simulation platform as a carrier, integrates model-driven simulation technology and massive multi-source power data, and designs a digital twin power system framework with multi-dimensional data space and multi-physical field under virtual-real interaction.

2.1 System framework

The new power system digital twin framework constructed in this paper is shown in Fig. 1, including five layers: physical layer, transmission layer, model layer, platform layer, and service layer.

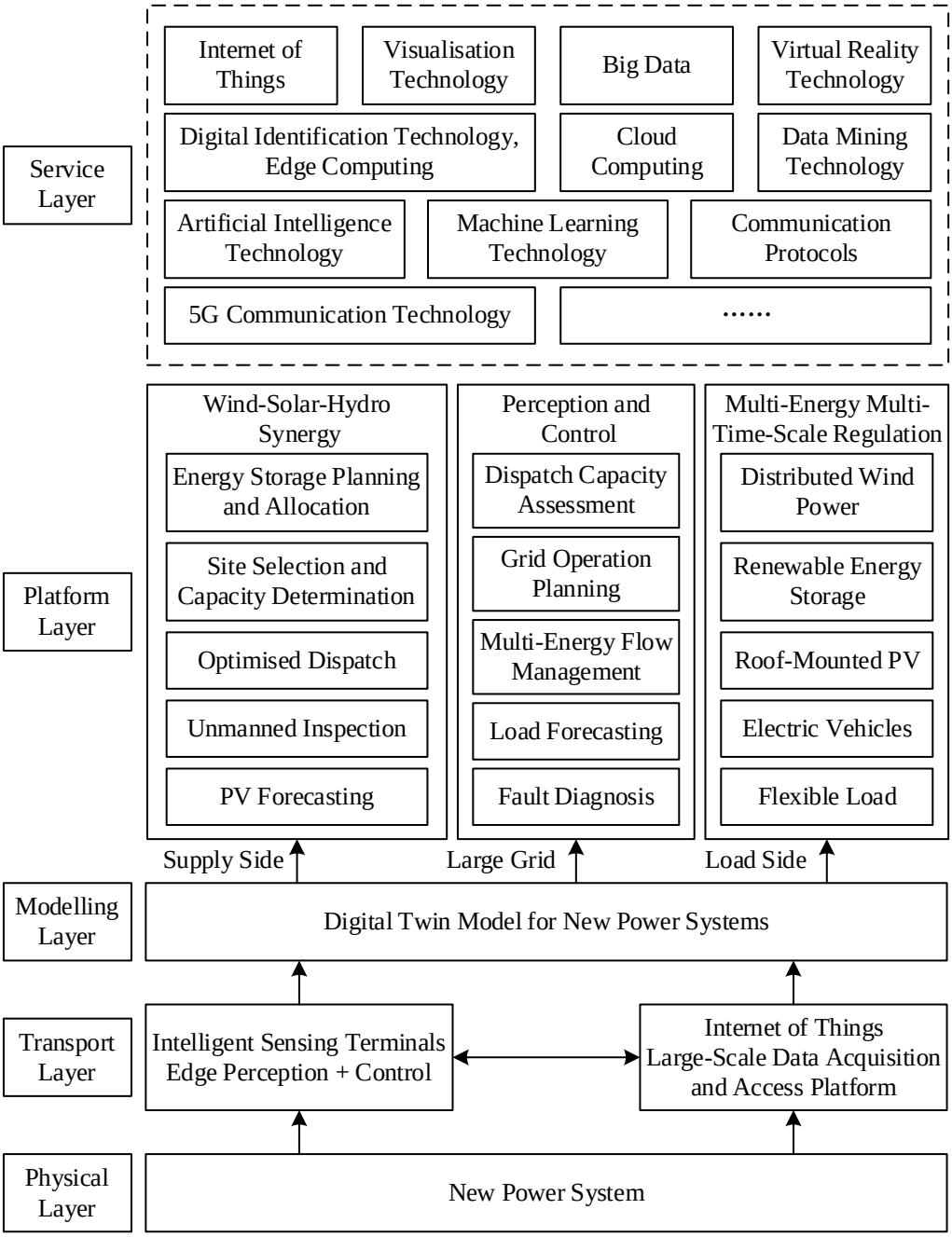

Figure 1: Digital twin framework of the new power system

(1) The physical layer includes all the equipment in the new power system such as wind farms, photovoltaic power plants, hydroelectric plants, substations, converter stations, transmission lines, and energy storage devices.

(2) The transmission layer, on the other hand, includes a huge number of sensors and intelligent sensing terminals to accurately collect data from the physical layer for planning and designing, offline training, and online updating of the digital twin model of the new power system.

(3) The model layer needs to deeply explore the intrinsic mechanism of the new type of power system after the access of large-scale new energy, power electronic equipment, and new type of loads, and establish electromechanical transient, electromagnetic transient, current model, optimal scheduling, demand response and other models in line with the characteristics

of the new type of power system.

(4) The platform layer is to build a digital platform on the basis of the model, which is the digital carrier of the data-physical fusion model, and at the same time is the interface platform for various power services.

(5) The service layer is a cloud platform constructed on the basis of emerging information technologies and digital technologies such as big data, cloud computing, edge computing, deep learning, etc., which is the medium of communication between the entire digital twin power system and the market and users.

2.2 System modeling

In this paper, a digital twin model of a novel power system is proposed using data-physical fusion modeling method as shown in Fig. 2, where MPC is the secure multiparty computing protocol.

The new power system digital twin model is an organic coupling of the physical simulation model and the operational state data model, both of which are independently trained offline and cooperatively run online. Ideally, the output of the digital twin system will track the output of the physical system in real time. Physical models are simplified mathematical equivalent models obtained after in-depth study of the physical world, which are generally built under certain assumptions and constraints, whereas data-based models capture the behavioral characteristics of physical phenomena from a large amount of data. For physical models, data models can complement the physical features of the unmodeled and unmodelable parts and correct the results of physical models.

The twin data is the real-time output data of the digital twin system, which interacts downward with the real-time sensing data of the new power system, updates and optimizes the data model parameters online, and provides data upward to the cloud service platform for completing the upper layer of business, such as peak-fill-peak and power trading. At the same time, the digital twin system needs to have a flexible system data interface to access information from the data collection and monitoring control system (SCADA), engineering production management system (PMS), order management system (OMS), etc., and be able to clean and merge the accessed data to form structured time-sequence data with business information.

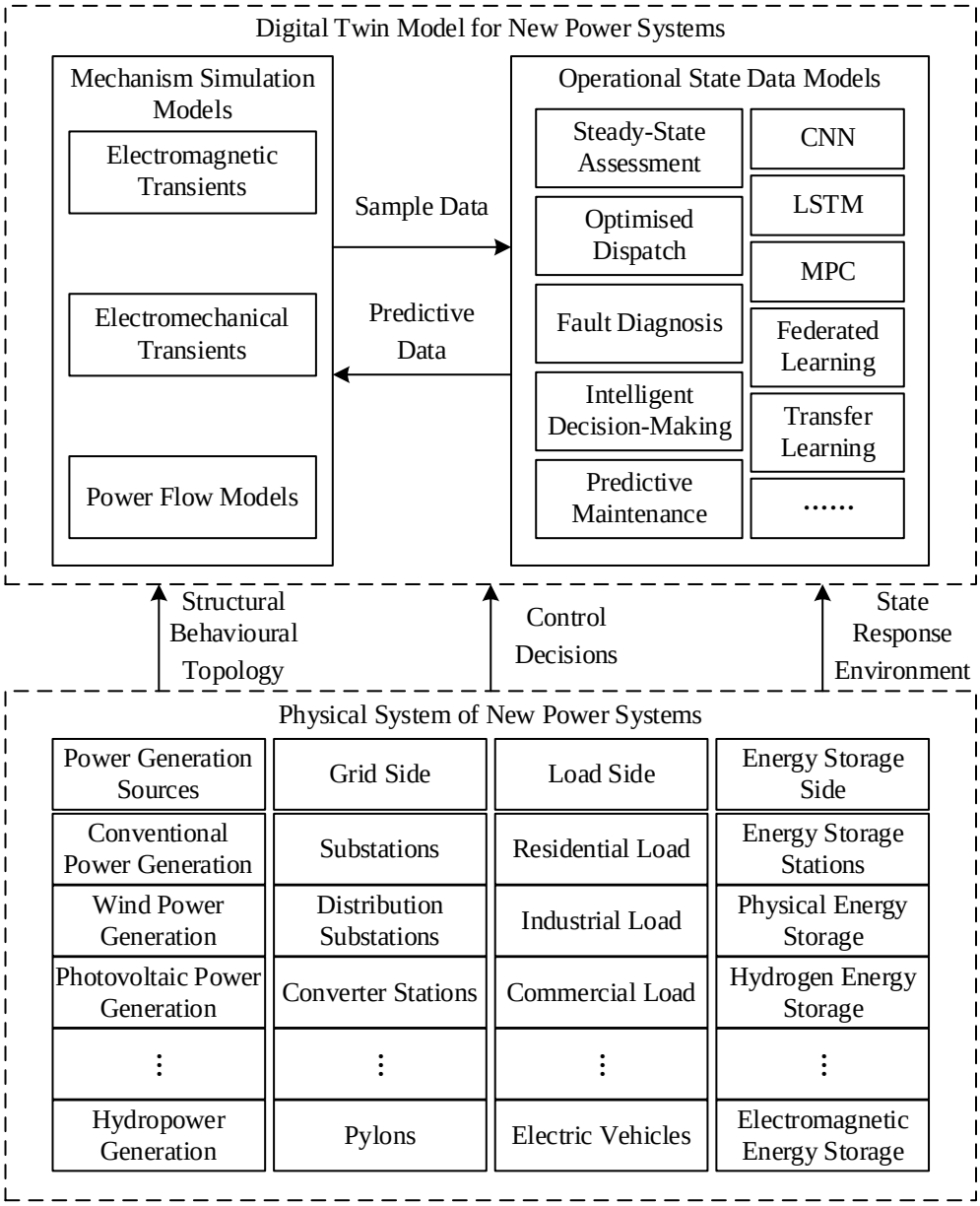

Figure 2: Digital twin model of the new power system

3 Data-physics fusion for dynamic analysis of power system frequency response

Based on the digital twin framework for power systems with data-physical fusion, this chapter explores a dual-drive dynamic analysis method for power system frequency response with data-physical fusion.

3.1 Dynamic process of frequency response at the beginning of the disturbance

When a frequency event occurs in the power system and causes the frequency to deviate from the normal value, its dynamic frequency process can be roughly divided into three phases, i.e., perturbation power distribution, inertia response, and FM measure response, and the

distribution of each phase on the time axis is shown in Fig. 3, where t_0 is the moment of perturbation occurrence, t_{gov} is the moment of governor action, and t_{nadir} is the moment corresponding to the lowest point of frequency.

When $t = t_0^+$, i.e., the transient instant after the perturbation occurs, the perturbation power distribution phase: the shock power will be distributed among the synchronous generators according to the synchronous power coefficients of each synchronous unit with the perturbation point, and the synchronous units electrically close to the perturbation point will share more of the shock power, independently of the generator's capacity and inertia size. Since it takes time for the generator speed to change, the rotational kinetic energy stored in the rotor at the moment $t = t_0^+$ does not provide the system with energy to cope with the disturbance power. In fact, at this stage, the electromagnetic energy stored in the generator is released to temporarily act as "emergency energy", which is manifested as a transient change in the electromagnetic power of the synchronous unit at the moment of the disturbance. Compared with the synchronous machine, the renewable energy unit lacks the power angle characteristics and cannot share the disturbance power according to the synchronous power coefficient, so the only remaining synchronous unit in the new energy grid with a high proportion of new energy will share a larger shock power, and the vulnerability of the grid will be further increased.

When $t_0^+ < t < t_{gov}$, i.e., after the perturbation appears until the start of one FM, the pure inertia response stage: the perturbed power has been allocated for the first time, for example, in the case of shock load, the electromagnetic power of synchronous unit instantly becomes bigger, but its mechanical power does not change, and the generator rotational speed is easily known to be decreasing according to the equation of motion of the rotor, and the rotational kinetic energy stored on the generator rotor will be released partly to the power system to offset the power deficit caused by the shock load. In this process, the rotational kinetic energy stored in the generator rotor will be released partly to the power system to offset the power deficit caused by the shock load, the process is the inertia response. Therefore, it is not difficult to find that the essence of inertial response is the rotational kinetic energy of synchronous networking equipment or other forms of energy storage in the disturbance to inject or absorb energy into the power system, so that the supply and demand of active power in the grid to maintain balance again. However, inertial resources are not sustainable energy, their capacity is only as much as the inertial source can store, and the rotational kinetic energy is proportional to the square of the rotor speed, so the inertial source releases energy accompanied by a drop in rotational speed, which in turn causes a drop in the grid frequency.

When $t_{gov} < t < t_{nadir}$, i.e., after the governor action until the frequency reaches the lowest point, the inertia response and the primary frequency regulation stage: governor action, the generator's mechanical power will increase, the difference between the mechanical power and the electromagnetic power will be reduced, based on the rotor equations of motion it is not difficult to find that the generator speed reduction rate will be Decrease, at this time associated with the grid frequency drop began to slow down. As the governor response power is getting bigger and bigger, the inertia response of the force will start to reduce, until the governor response power and disturbance power is equal, the inertia response is no longer out of force, the system frequency is no longer declining, that is, the frequency has reached its lowest point. Before the frequency reaches the minimum point, the inertial response can still play a positive role in regulating the system frequency to enhance its anti-disturbance capability. However, after the lowest point in frequency, the dominant role in frequency regulation is a frequency adjustment, and inertia response has become a "burden", the frequency of the recovery process is actually the system for the inertia source "energy" process.

Therefore, the assessment of the system inertia level is of great significance, the lack of inertia will bring security risks for the system, while excess inertia will not only bring economic waste, but also increase the system's "inertia", affecting the regulation effect of other means of frequency regulation.

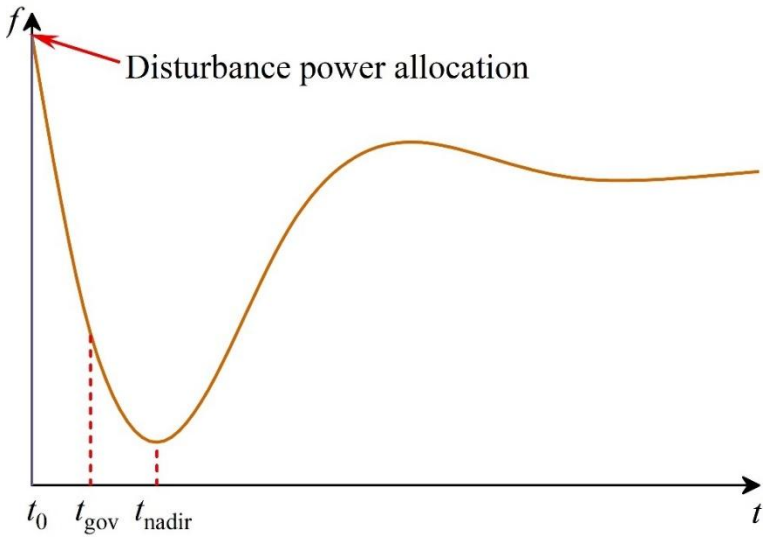

Figure 3: System dynamic frequency response curve

3.2 Analysis and improvement of power system frequency response modeling methods

In this section, based on the modeling idea of "Critical Factor Physical Model-Non-Critical Factor Data Model", its application in the online posture analysis of power grid frequency is investigated.

3.2.1 Physical simplified model for frequency posture prediction

Currently, the frequency posture prediction methods applied on-line are mainly the single-engine equivalent modeling method represented by SFR. This type of method equates the whole network generator/load model into a single machine with centralized load model. In the physical-data fusion modeling method proposed in this paper, the choice of physical model has better flexibility, and the SFR model is used as a simplified physical model in this study. It should be noted that in the proposed physical-data fusion modeling approach, the physical model can also be replaced by the improved frequency response model mentioned above.

Using the perturbation power P_d to represent the change in the unbalanced power of the system as an input to the model, the SFR model can be expressed by the following equation:

$$\Delta\omega = \left(\frac{R\omega_n^2}{DR + K_m} \right) \left(\frac{(1+T_g s)P_d}{s\left(s^2 + 2\zeta\omega_n s + \omega_n^2\right)} \right) \tag{1}$$

Among them:

$$\omega_n^2 = \frac{DR + K_m}{2HRT_g}$$
$$\zeta = \left(\frac{2HR + (DR + K_m F_H)T_g}{2(DR + K_m)} \right) \omega_n \tag{2}$$

where H is the equivalent inertia time constant, D is the equivalent damping coefficient, R is the equivalent system modulation coefficient, F_H is the equivalent reheat unit high-pressure cylinder capacity coefficient, T_g is the equivalent reheat time constant, K_m is the rotating standby capacity and the system power factor related constants, P_d is the power deficit and $\Delta\omega$ is the frequency deviation value.

The prerequisite for the application of the SFR model method is to equate the complete system containing all the units into a single-unit system. In this paper, according to the theory of transformation of the system's center of inertia, all the units in the system are merged and the role of the system network is ignored, so as to normalize and calculate the parameters of the single-unit system.

3.2.2 System Frequency Response Correction Modeling

For the power system frequency stability problem, the most important factors determining the frequency response characteristics of the system after disturbance are the inertia, damping and speed regulation characteristics of the system composed of generating units and loads, and in the study of this paper, this part of the main influencing factors is regarded as the key factors for the study of the frequency stability problem. The grid structure, voltage reactive power dynamic characteristics, etc. also have a slight impact on the system frequency posture, and these secondary influences are regarded as non-critical factors in the study of the frequency stability problem.

For the key factors, the computational analysis method based on the simplified equivalent of the actual system represented by the SFR model method can roughly obtain the frequency trajectory curve of the system after disturbance. Therefore, this physical simplified model is considered to retain the more obvious physical connection between the input and output data of the power system frequency stabilization problem.

In order to further improve the computational accuracy of the frequency response model represented by the SFR model, a machine learning method is considered to be used to combine various types of secondary factors, and a system frequency response correction model based on the machine learning method is proposed.

The construction and application of the system frequency response correction model is shown in Fig. 4, which includes the physical simplification model as well as the prediction error correction model. Among them, the physical simplified model SFR, which is used in this paper, is constructed based on the mechanism of the influence of the key factors on the frequency dynamics, and takes the information such as the description of perturbation events and power system topology/parameters as inputs. The inputs of the prediction error correction model are the predicted frequency dynamics of the physical simplified model and the wide-domain measurement information of the non-critical factors, and the output is the real frequency dynamics, which is established after the offline training of the sample data by the machine learning method.

In practice, the core of the system frequency response correction model lies in the coordination mechanism between the physical simplified model and the prediction error correction model: the physical simplified model firstly predicts the frequency potential based

on the event description and power system topology/parameter information, and its prediction results together with the wide-area measurement information of the non-critical factors serve as inputs to the prediction error correction model, which in turn outputs the final frequency potential.

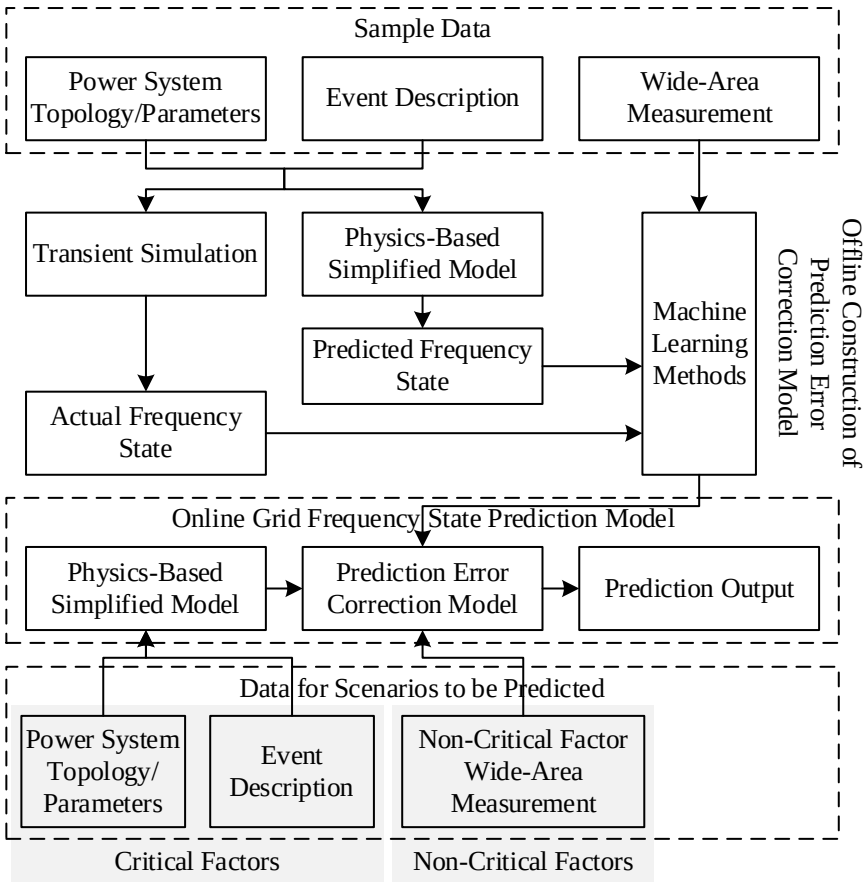

Figure 4: Construction and application of system frequency response correction model

3.3 Data-physics fusion based frequency response analysis methods

3.3.1 Methods for Integrating Physically-Driven and Data-Driven Models

At present, there are four typical joint modes of data-physical fusion driving methods applied in various scenarios of power system applications: parallel mode, bootstrap mode, serial mode, and feedback mode.

Since the actual demand of frequency response analysis is to accelerate the calculation speed and ensure the prediction accuracy, this paper adopts the serial mode to fuse the two models. The data-driven model is used to study the correlation between the output data of the simplified physical-driven model and the actual results in different scenarios, which in turn realizes the use of the data-driven model to correct the results of the initial measurement data of the physical-driven model.

3.3.2 Frequency response analysis method based on fusion modeling

In order to achieve a more accurate and efficient frequency response analysis algorithm, this paper considers a deep learning model capable of analyzing time series type data and incorporating power system instantaneous time series datasets to correct the SFR model error.

As a result, a fusion model with the attention mechanism-based two-branch network model (TBNAM) as a data-driven approach is proposed.

In order to preserve the electrical causality between the input and output data of the power system frequency stabilization problem, this paper uses the SFR model as a physically driven method. With this model, the frequency change curve of the system after the disturbance can be obtained and the key features for frequency stability evaluation can be extracted. These key features and the system transient timing dataset are jointly used as inputs to the two-branch network model based on the attention mechanism to complete the serial-mode based fusion model. The schematic structure of the fusion model is shown in Fig. 5.

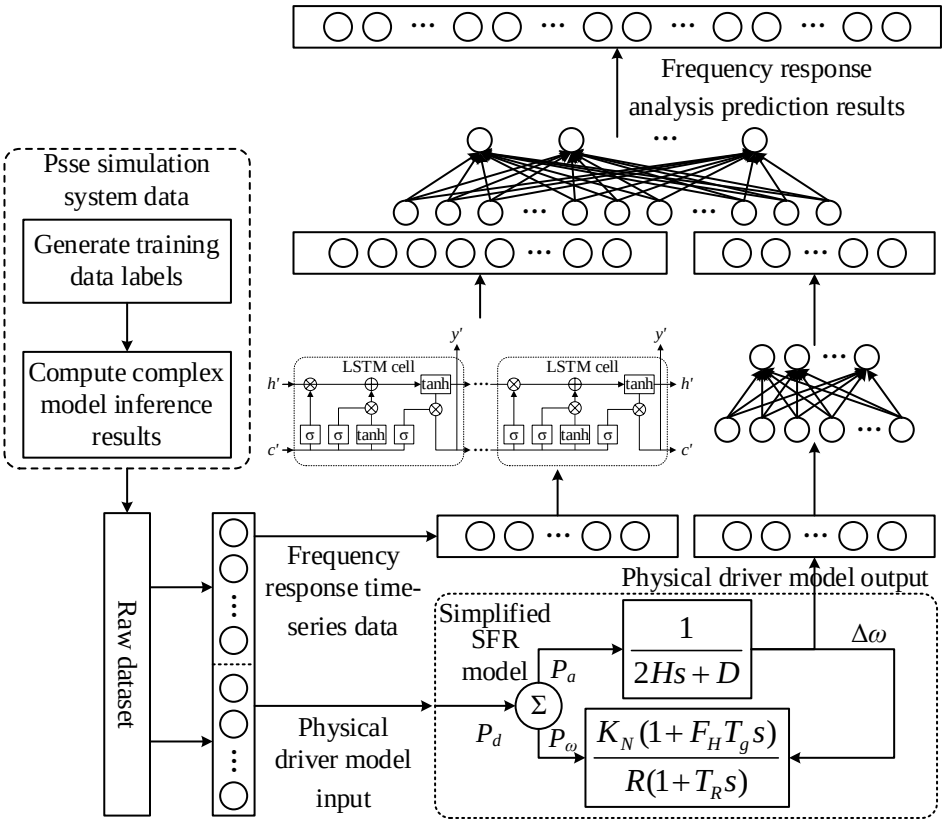

Figure 5: Structure of the fusion model

The structure of the two-branch network model based on the attention mechanism proposed in this paper is shown in Fig. 6, which consists of an input layer, an ordinary data feature extraction layer, a time-series data feature extraction layer, a feature fusion layer, and an output layer.

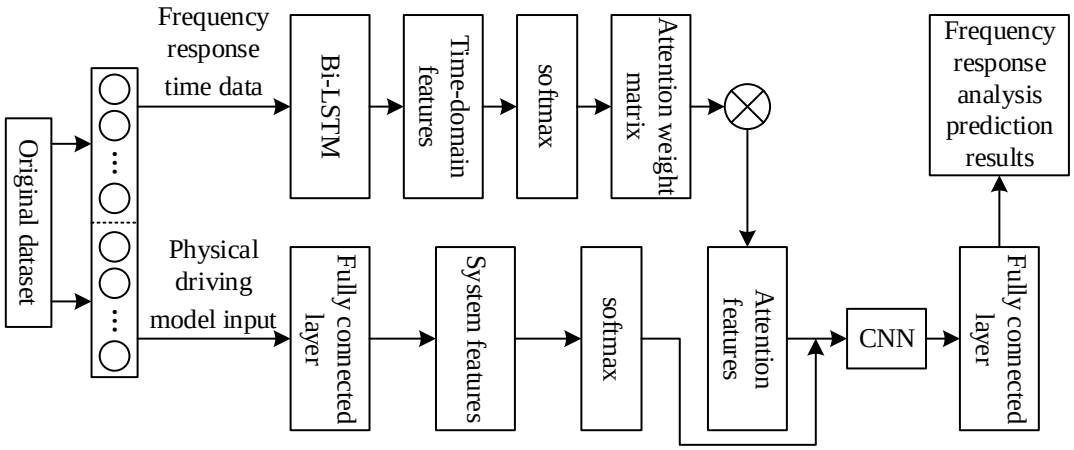

Figure 6: Dual-branch network structure based on attention mechanism

(1) Timing feature extraction layer

The timing data feature extraction layer will use Bi-LSTM, attention mechanism and CNN to extract deeper timing features from the frequency response timing data.Bi-LSTM uses one memory unit and three gating units to extract timing features at the current moment, and decides to retain the information of the memory module of the hidden layer unit up to the current moment through the two-layer network layer. The parameters of the three gating units at the current moment t are calculated as follows:

$$f_t = \sigma\left(W_f \cdot [h_{t-1}, x_t] + b_f\right) \tag{3}$$

$$i_t = \sigma\left(W_i \cdot [h_{t-1}, x_t] + b_i\right) \tag{4}$$

$$o_t = \sigma\left(W_o [h_{t-1}, x_t] + b_o\right) \tag{5}$$

where W and b are the weight matrix and bias vector to be learned during training, x_t is the input at moment t, h_{t-1} is the output at moment $t-1$, and σ is the Sigmoid function. $\tilde{C}_t$ is the new alternative cell state, C_t is the cell state at moment t, C_{t-1} is the cell state at moment $t-1$, and the cell state at moment t, C_t, is updated by $\tilde{C}_t$ and C_{t-1} together, which is calculated as follows:

$$C_t = f_t * C_{t-1} + i_t * \tilde{C}_t \tag{6}$$

$$\tilde{C}_t = \tanh\left(W_c \cdot [h_{t-1}, x_t] + b_c\right) \tag{7}$$

where W and b are the weight matrix and bias vector to be learned during the training process, and * is the matrix element inner product operation. Finally, the output o_t is obtained by two network layers layer deciding to retain the information of the memory module of the hidden layer unit up to the current moment, and the t moment output h_t is obtained:

$$h_t = o_t * \tanh\left(C_t\right) \tag{8}$$

Bi-LSTM consists of two layers of LSTMs trained in both forward and reverse directions, and they are spliced together so that the state at the current moment can take into account information from both the front and back directions. As a result, the output matrix is computed as follows:

$$H = \left[\vec{H} * \overleftarrow{H} \right] \tag{9}$$

where $\vec{H} = \left\{ \vec{h}_1, \vec{h}_2, \cdots, \vec{h}_T \right\}$, $\overleftarrow{H} = \left\{ \overleftarrow{h}_1, \overleftarrow{h}_2, \cdots, \overleftarrow{h}_T \right\}$, * for the matrix element inner product operation.

Afterwards, the output matrix H is converted into a frequency response time series representation using the attention mechanism. The attention mechanism is capable of dynamically selecting important information and focusing on it, so the mechanism assigns different weights to each moment vector in the matrix H according to the importance of the information at key time points in the timing data in order to capture the important timing information in the system's electrical volume data. Since the output h_m of the last moment in Bi-LSTM contains all the information in the timing data, this paper uses the attention mechanism to obtain the timing data representation p by performing the following equation:

$$\alpha = soft\max\left(H^T W_a h_m \right) \tag{10}$$

$$p = \tanh\left(W_p H \alpha + W_p h_m + b_p \right) \tag{11}$$

where W_a is the attention weight matrix, α is the weight vector, and W and b are the in-weight matrix and bias vector.

(2) Fusion of physical driving model features with timing features

In order to fuse the time-series features with the physical-driven model features, the time-series representation p is first processed using a 1-dimensional convolution kernel, which is calculated as follows:

$$o[n] = f[n] * g[n] = \sum_{m=-\infty}^{\infty} f[m] g[n-m] \tag{12}$$

where o is the convolution output, f and g are the convolution input and convolution kernel, and * is the convolution operation.

The 1-dimensional convolution inputs are vectors, so the time-series data are vectorially spliced $x = [x_1, x_2, \cdots, x_n]^T$, and the convolution kernel window is defined as r , and the features are obtained by the convolution operation, which is calculated as follows:

$$c_i = f\left(w^T * x_{i:j+r-1} + b \right) \tag{13}$$

where $x_{i:i+r-1}$ is the column-first grand vector spliced from i to $i+r-1$ vectors, b is the bias vector, and f is the activation function. This yields an equal-width convolutional feature representation $c = [c_1, c_2, \cdots, c_n]$. After that, in order to fuse with the output of the physical driver model, the equal-width convolutional features are subjected to global max-pooling, and the high-dimensional features are compressed to obtain one-dimensional features, and the max-pooling formula is as follows:

$$\hat{c}_i = \max\left\{c_i; c_{i+r-1}\right\} \tag{14}$$

where r denotes the pooling step and $\hat{c}$ denotes the pooled features. Finally, the vector $\hat{c}$ and the SFR model output f are spliced to obtain a vector v of fusion of physically-driven model features and timing features:

$$v = \left[\hat{c}, f\right] \tag{15}$$

(3) Frequency Response Analysis and Prediction

Finally, in order to improve the model prediction accuracy, the vector v is used with a fully connected layer as well as the ReLU activation function to obtain the characteristic vector v' for final testing:

$$v' = \mathrm{Re}\,LU\left(W_v' v + b_v'\right) \tag{16}$$

where W, b are in weight matrix and bias vector.

And the final tested characteristic vector v' is predicted for frequency response analysis using the fully connected layer, and the frequency response analysis prediction result o is obtained:

$$o = W_o v' + b_o \tag{17}$$

where W and b are the in-weight matrix and the bias vector.

4 Simulation Verification and Example Analysis

4.1 Data-driven model training

Building the data-driven model TBNAM proposed in this paper requires data from various transient scenarios for training, whereas the probability of failure scenarios in actual operation is extremely low and it is difficult to collect data from various transient failure scenarios, so Matlab software is used for simulation.

The constructed model is based on PSAT toolkit and the model is based on the improved IEEE14 node model. On the basis of the original IEEE14 node model, a wind farm model based on the PSAT software package consisting of multiple doubly-fed wind turbine equivalents is added at bus node 1, and a photovoltaic (PV) power generation system model is added at bus 3. The fault type set is a three-phase short circuit, the location is near bus 6 on the line from bus 6 to bus 12, and the simulation system runs realistically for 8s.

A large amount of training data is obtained by setting different scenarios, and the calculation step size of the time-domain simulation method is set to 0.0005s, and a total of 101,254 sets of training data are obtained by setting the random fault duration, random generator output, random wind speed, random load fluctuation, and extracting the input and output variables of the differential equation set calculation module of the wind power model and the photovoltaic model.

(1) Equal-step data-driven model training

The inputs and outputs of the data-driven model of the wind turbine are the input variables and output variables of the differential equation system calculation module in the wind turbine model, respectively. The data-driven model input and output data of the photovoltaic power

generation system are consistent with the wind turbine. The obtained 101254 sets of wind turbine and photovoltaic power generation system differential equation system data are inputted into the data-driven model for training, and the TBNAM equal-step-length data-driven model of the differential equation system in the wind turbine and photovoltaic power generation system is obtained.

(2) Cross-step data-driven model training

In this paper, 0.0005s is selected as the time step of the power electronic equipment in the system, while the generator time domain simulation often adopts 0.01s as the time step, so n=20 is taken, which can make the power electronic equipment in the time domain simulation have an accuracy close to the 0.0005s step, and at the same time, the computation step is changed to 0.01s, so that the power electronic equipment is consistent with the accurate computation step of the other components. All of them are 0.01s, which makes it easy to realize the mixed driving of data model and physical model in each step.

Next, we verify the influence of n value on the accuracy, and choose to observe the change rule of n value under the transient instability scenario with relatively large error, and the change rule of generator power angle error with n value is shown in Fig. 7. Where, (a) indicates the change of error with time at each n value, and (b) indicates the relationship between the maximum error and n value.

It can be seen that if the maximum error threshold of 12% is taken, the accuracy requirement is satisfied when n=32 or less, and in this paper, taking n=20 can ensure higher accuracy. The output variables of the differential equation system calculation module of the wind turbine and photovoltaic power generation system are processed respectively, and the output value of each step is changed to the average of the output values of the last 10 small step lengths by the stepwise Euler method, and the stepwise data-driven model training data of the differential equation system in the wind turbine and photovoltaic power generation system are obtained after processing.

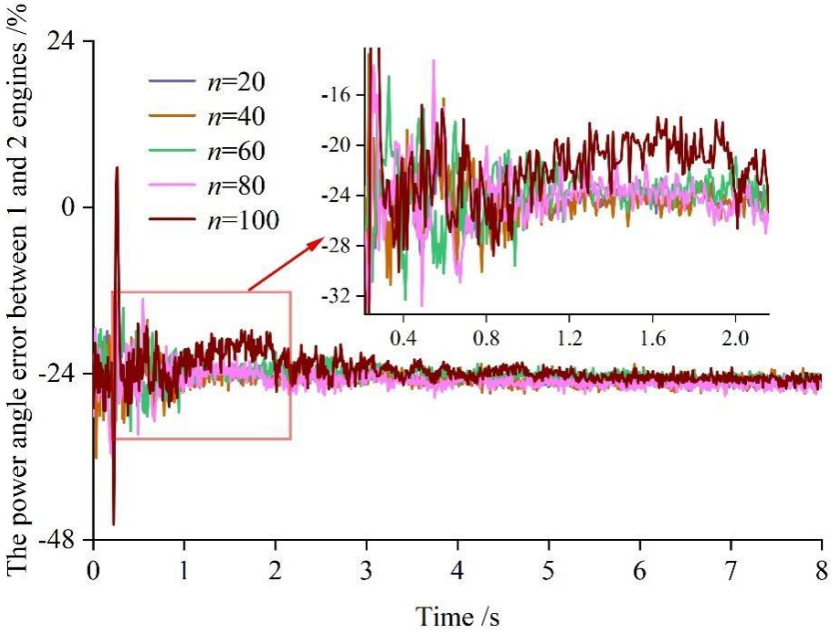

(a) The error under each n value varies with time

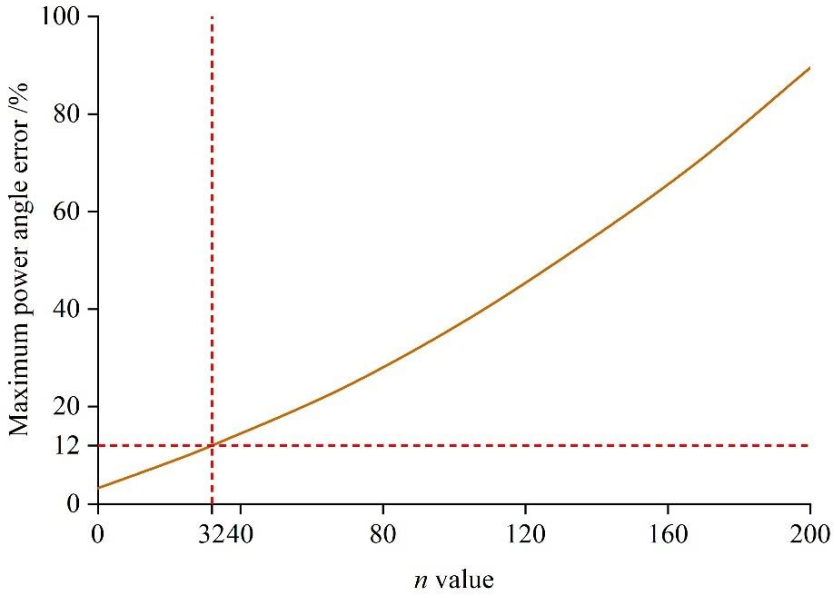

(b) Relationship between the maximum error and the value of *n*

Figure 7: The law of the generator's power Angle error varying with the n value

In addition, the following measures are taken to solve the error of the output data at the moment of short-circuit fault and fault removal:

(1) In the event of a short-circuit fault or fault resection, the calculation step of the time-domain simulation method is recalculated from this moment to obtain a more accurate value at the moment of system state change.

(2) Set the error threshold, near the moment of fault, to adaptively shorten the calculation time step.

4.2 Accuracy verification

The Polish-2383 nodal system is introduced, and 1 to 10 generators are arbitrarily selected in the improved IEEE14 and Polish-2383 nodal system to use the TBNAM data-driven model, and the rest of the generators are still using the improved physical model of SFR based on the system's frequency response correction model (ISFR), and in this paper's validation, the generators use the second-order model, and the step size of the simulation is is set to 0.01s and the convergence criterion e=105.

The time-domain simulation results obtained by using the proposed data-physical fusion driving method (TBNAM-ISFR) tested in the IEEE14 and Polish-2383 node systems are shown in Fig. 8 and Fig. 9, respectively. In particular, the fault initiation time is 0.24s and fault removal time is 0.30s in the IEEE14 system, while in the Polish-2383 system it is 0.24s and 0.40s, respectively. (a)~(d) denote the time-domain simulation results of power angle δ_1 and nodal voltage magnitude of generator 1, as well as the relative errors of power angle and voltage magnitude with respect to the simulation results of the Power System Analysis Tool (PSAT), respectively.

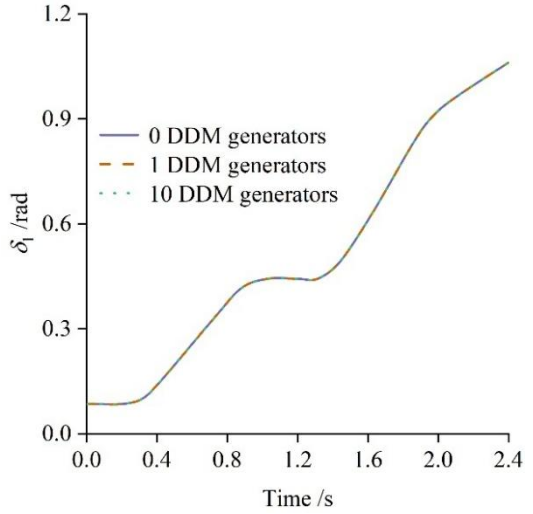

(a) Power angle δ_1

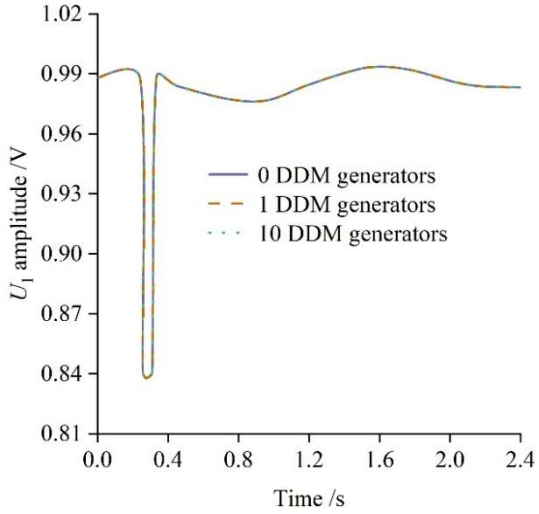

(a) U_1 amplitude

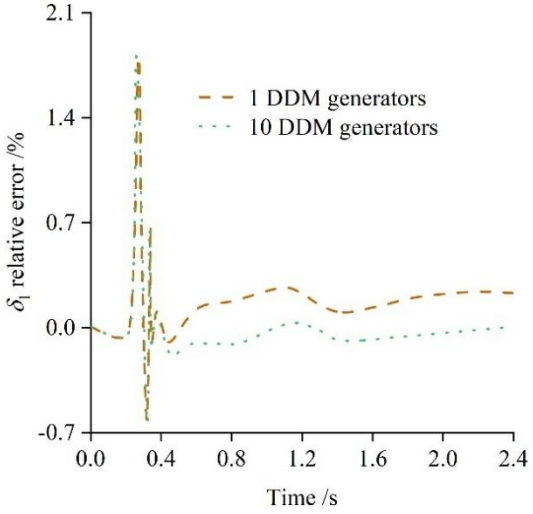

(c) δ_1 relative error

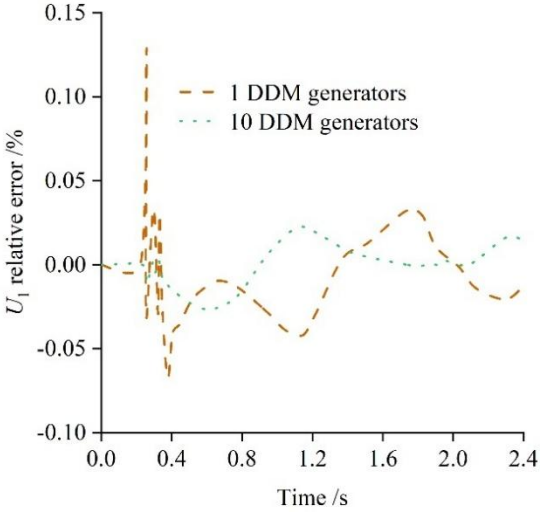

(d) U_1 amplitude relative error

Figure 8: Time-domain simulation results of the IEEE14 node system

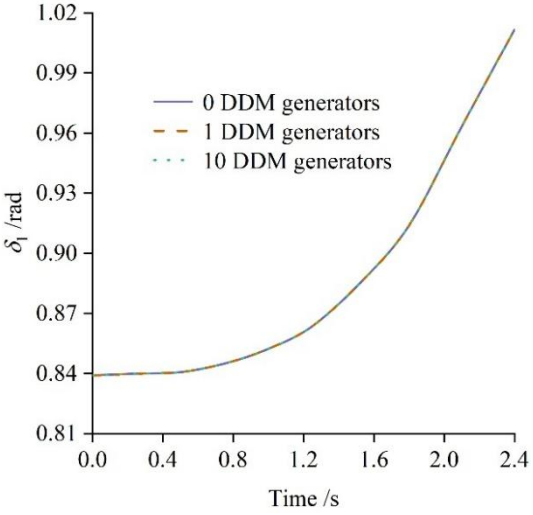

(a) Power angle δ_1

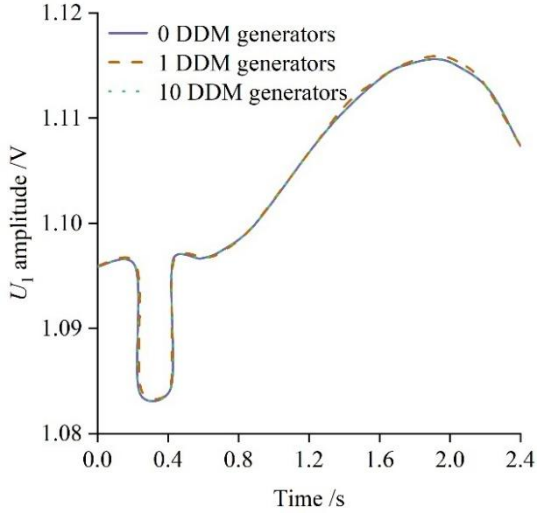

(a) U_1 amplitude

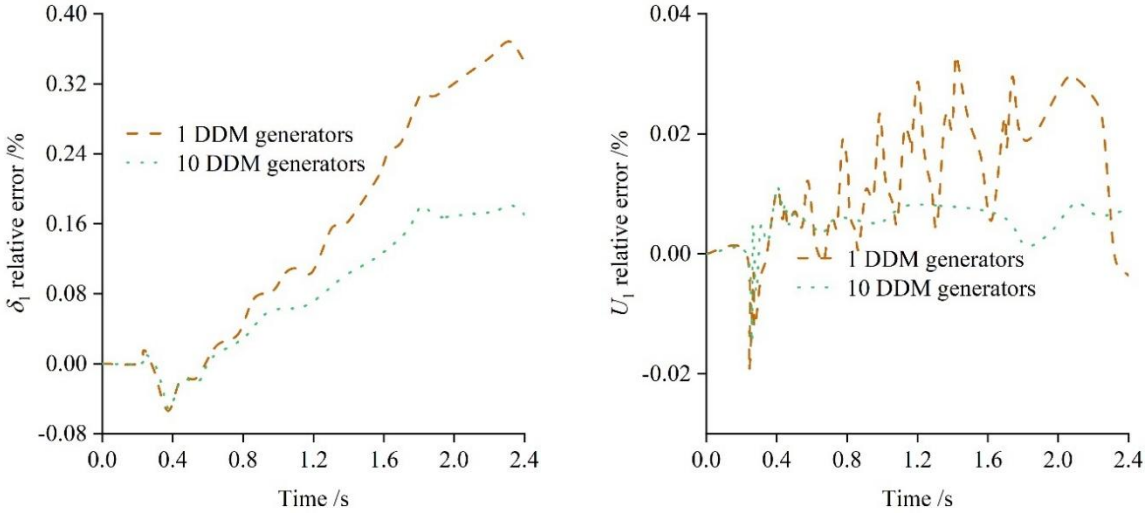

(c) δ_1 relative error (d) U_1 amplitude relative error

Figure 9: Time-domain simulation results of the Polish-2383 node system

In order to further illustrate the effectiveness of the proposed data-physical fusion-driven simulation algorithm TBNAM-ISFR, the load size and generator output are set to vary randomly within the range of ±25%, and 24 initial operating points different from the training set are obtained through the tidal current computation, and 10 lines are extracted from the system for the three-phase short-circuit experiments, and the values of the grounding resistances are set to be 1.2×10^{-3} and 1.2×10^{-6}, and the fault duration ranges from 0.01 to 0.37s, with a total of 10 at 0.04s intervals, forming a total of 4800 fault scenarios that are different from the training set, and taking the PSAT simulation results y_{psat} as the reference standard, the following formula is used to calculate the average of the variables y_{sim} obtained from the simulation of the proposed methodology Relative error e:

$$e = \left[\sum_{i=1,j=1}^{i=N,j=L} \left| \left(y_{sim}^{ij} - y_{psat}^{ij} \right) \Big/ y_{psat}^{ij} \right| \right] \Big/ \left(N \times L \right) \tag{18}$$

where: N denotes the number of variables in the same category. L is the number of time points in a single simulation.

The relative error results of the simulation results of the 2 validation systems are shown in Table 1.

Table 1: Relative error of simulation results

Variable	Relative error /%			
	One DDM generator		10 DDM generators	
	IEEE-14	Polish-2383	IEEE-14	Polish-2383
δ	2.681	0.243	0.442	1.245
I amplitude	0.284	0.045	0.077	0.159
I phase angle	2.895	0.078	0.080	0.118
U amplitude	0.032	0.003	0.020	0.021
U phase angle	1.743	0.079	0.022	0.004

The results in Figures 8~9 and Table 1 show that the proposed algorithm can be effectively applied to the electromechanical transient simulation of power systems with data-physics fusion-driven modeling. Regardless of whether some or all generators in the system are modeled with data-driven modeling, the results of each state variable and operation variable in the system can be accurately obtained, which are basically consistent with the PSAT reference results.

4.3 Generalizability test

By changing the fault location and fault time, several sets of fault scenarios are set up to test the accuracy of the hybrid-driven time-domain simulation method of the data-driven model and physical-driven model proposed in this paper under each scenario. According to the different scenarios and algorithms, the simulation data are classified into four categories: cross-step instability, equal-step instability, cross-step stabilization, and equal-step stabilization, and Eq. (19) is used to obtain the average absolute error index to verify the accuracy of the proposed method:

$$M = \frac{1}{mn}\sum_{j=1}^{m}\sum_{i=1}^{n}\left|x_{ij} - x_{real}\right| \tag{19}$$

where: M is the mean absolute error. m is the number of lines, nodes or generators. n is the number of steps. x_{ij} is the simulation data of the method proposed in this paper. x_{real} is the real data.

The average absolute error of the method under each scene is shown in Fig. 10. As can be seen from the multi-scenario simulation results, the average absolute error of the power angle under each scenario does not exceed 1.40%, and the average absolute error of the voltage magnitude does not exceed 0.22%. Among them, the power angle error under the transient instability scenario is relatively larger compared with the transient stability scenario, which is due to the drastic change of the power angle of the partially unstabilized generator after the instability. Compared with the equal-step method, the error of the step-length method is relatively larger, which is because the step-length method skips the frequent fluctuation of the calculated values of small steps. It is thus verified that the data-driven model established in this paper is an internal driven model of power electronic components, which has good generalization ability and can meet the computational needs of various scenarios.

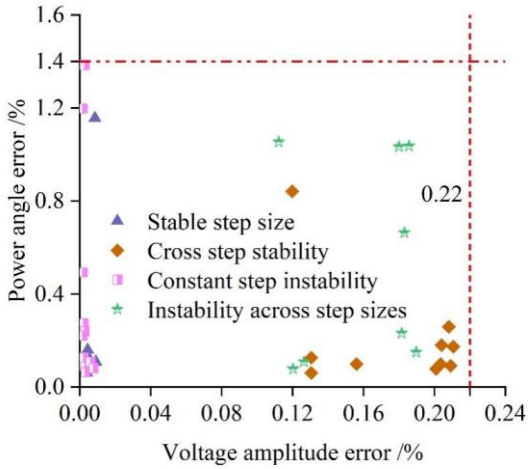

Figure 10: Mean absolute error of voltage amplitude and power angle in each scenario

4.4 Analysis of examples

In this section, the improved IEEE14 node system and the actual system of Fujian Power Grid are used as the simulation system, and the PSD-BPA simulation platform is utilized to build the model for dynamic simulation. In order to verify the effectiveness of the proposed model in terms of performance enhancement, the prediction results of the physical model, data-driven model, and fusion model are compared in the simulations in this section. The performance evaluation and error analysis are based on the prediction results of minimum frequency, steady state frequency, and extremum time.

4.4.1 IEEE14 Node System

(1) Minimum Frequency Prediction

A comparison of the minimum frequency prediction results for the physical, data-driven, and fusion models is shown in Table 2.

It can be seen that there are significant accuracy differences between the physical, data-driven, and fusion models Specifically, among the above models, the SFR model has the largest overall error. It can be seen that in practical applications, it is difficult to obtain ideal prediction accuracy by directly using the traditional SFR model. Compared with the SFR model, the ISFR model has a significantly lower error level, proving the effectiveness of the ISFR model proposed in this paper. Unlike physical models, data-driven models utilize a large amount of system operation data for training. Therefore, the predictive performance of the TBNAM model is further improved compared to the ISFR model. Specifically, the MAE, MAPE, and RMSE of TBNAM are reduced by 0.00766 Hz, 7.192%, and 0.00953 Hz, respectively.This demonstrates the advantages of the TBNAM model as a data-driven model in feature learning and mapping fitting. In addition, the prediction accuracy of the fusion model is significantly higher than the other models. Among the fusion models, the TBNAM-ISFR model has the lowest prediction error with MAE, MAPE and RMSE of 0.000476Hz, 0.446% and 0.000554Hz, respectively.

Table 2: Minimum frequency prediction errors of different models

Model	MAE /Hz	MAPE /%	RMSE /Hz
SFR	0.0284	24.981	0.0349
ISFR	0.00961	8.975	0.0118
TBNAM	0.00195	1.783	0.00227
TBNAM-SFR	0.000917	0.847	0.00105
TBNAM-ISFR	0.000476	0.446	0.000554

Meanwhile, in order to further compare the prediction performance of the TBNAM model and the fusion model, 100 samples are randomly selected, and the absolute error comparison of their lowest frequency prediction is shown in Figure 11.

It can be seen that there is an obvious accuracy gap between the TBNAM model and the TBNAM-based fusion model, which indicates that the combination of data-driven and physical models can effectively improve the prediction accuracy. In addition, compared with the TBNAM-SFR model, the TBNAM-ISFR model has a smaller error amplitude and a lower level of error fluctuation, which proves the feasibility and effectiveness of introducing the ISFR model.

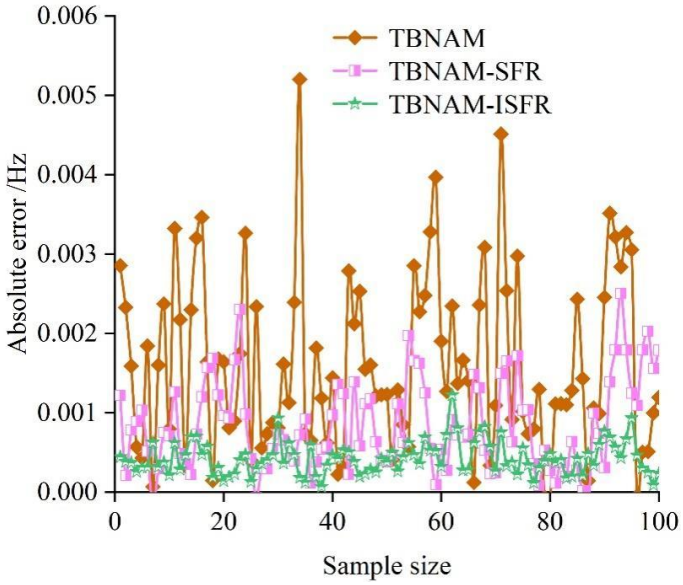

Figure 11: The absolute error of the lowest frequency prediction

In addition, the training time of the TBNAM-ISFR model is 102.70 s, and the prediction time is only 0.082 ms. Since the training is performed offline, the overall time taken by the TBNAM-ISFR model is perfectly acceptable.

(2) Steady-state frequency prediction

Comparison of the prediction results of steady state frequency by different models is shown in Table 3.The prediction accuracy of the ISFR model is much higher than that of the SFR model. Compared with the SFR model, the MAE, MAPE and RMSE of the ISFR model decreased by 0.01474Hz, 26.317% and 0.03592Hz, respectively, which provides a higher estimation accuracy of the steady state frequency.

Table 3: Steady-state frequency prediction errors of different models

Model	MAE /Hz	MAPE /%	RMSE /Hz
SFR	0.0179	32.184	0.0407
ISFR	0.00316	5.867	0.00478
TBNAM	0.00101	1.845	0.00126
TBNAM-SFR	0.000458	0.836	0.000578
TBNAM-ISFR	0.000229	0.421	0.000291

The absolute error of the steady-state frequency prediction is shown in Fig. 12.

Combining Table 3 and Fig. 12, it can be seen that the prediction results of the TBNAM model have been relatively accurate, but the accuracy of the TBNAM-SFR model still has considerable improvement. Specifically, the MAE, MAPE, and RMSE of the TBNAM-SFR model further decrease to 0.000458 Hz, 0.836%, and 0.000578 Hz.The above results indicate that the prediction performance can be further improved by combining the physical model with the data-driven model. Compared with the TBNAM-SFR model, the TBNAM-ISFR model further reduces the error metrics and shows better performance.The MAE, MAPE and RMSE of the TBNAM-ISFR model are 0.000229Hz, 0.421% and 0.000291Hz, respectively.In summary, the TBNAM-ISFR model can accurately predict the steady state frequency values and meets the accuracy requirements for online applications.

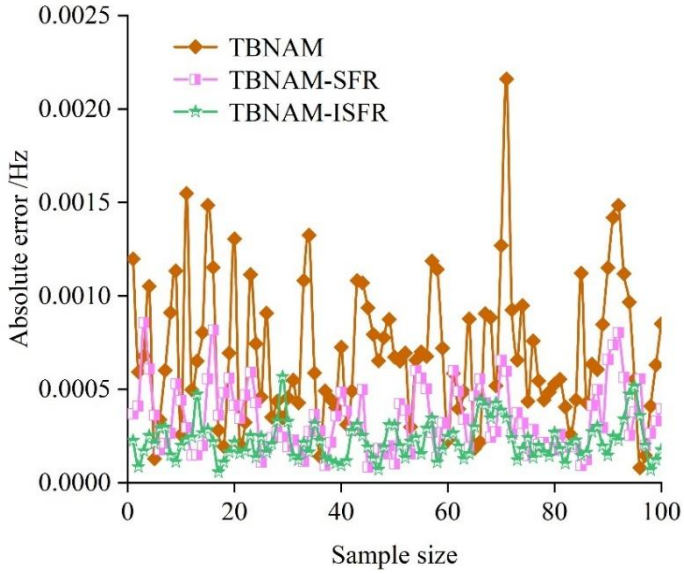

Figure 12: Absolute error of steady-state frequency prediction

(3) Extreme time prediction

The extreme time prediction results of each model are shown in Table 4. It can be seen that the error level of the SFR model is significantly higher than that of the other models.The MAE, MAPE and RMSE of the ISFR model are only 0.138s, 4.837% and 0.173s, which are significantly improved compared with the SFR model. Compared with the TBNAM model, the performance of the TBNAM-SFR model is further improved, but the improvement is limited. Take MAPE as an example. The difference in MAPE between the TBNAM model and the TBNAM-SFR model is only 0.284% when predicting the extreme value time, which is significantly smaller than 0.936% when predicting the minimum frequency and 1.009% when predicting the steady state frequency. The main reason is that there is a strong correlation between the extreme time and the system operation data. Meanwhile, the TBNAM model has a significant advantage in capturing time series features. Therefore, high prediction accuracy can be obtained by the TBNAM model alone.

Table 4: The extreme time prediction errors of different models

Model	MAE /s	MAPE /%	RMSE /s
SFR	0.597	21.025	0.749
ISFR	0.138	4.837	0.173
TBNAM	0.0246	0.892	0.0321
TBNAM-SFR	0.0174	0.608	0.0216
TBNAM-ISFR	0.00198	0.0719	0.00248

The absolute errors of the extreme time prediction are shown in Fig. 13. Combining Table 4 with Fig. 13, it can be seen that TBNAM-ISFR still has the best prediction performance in the prediction of the extreme time, with the model's MAE, MAPE, and RMSE of 0.00198s, 0.0719%, and 0.00248s, respectively.

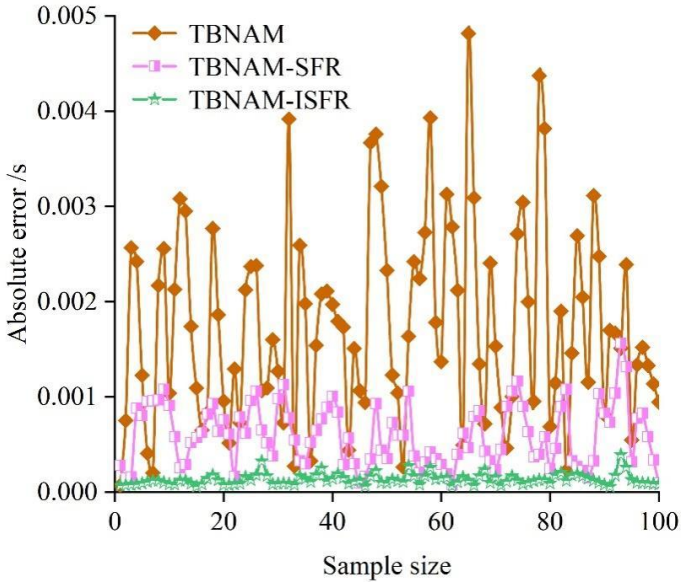

Figure 13: The absolute error of extreme time prediction

(4) Impact of sample size

In practical applications, sufficient samples are crucial for model training. In order to test the robustness of the prediction model to the sample size, the number of samples is reduced by a certain proportion for testing. The test results of each model are shown in Fig. 14, where (a) to (c) denote the MAE values of the minimum frequency, steady state frequency, and extreme time, respectively.

It can be seen that the MAE values of the TBNAM model increase significantly as the samples are reduced. Compared with the TBNAM model, the TBNAM-SFR and TBNAM-ISFR models show better performance, with smaller error fluctuations caused by changes in sample size. Among them, the TBNAM-ISFR model has the best robustness. The model has the largest error when the number of samples is scaled down to 360, and the MAEs for predicting the minimum frequency, steady state frequency, and extremum time are 0.00176 Hz, 0.000766 Hz, and 0.00937 s, respectively. In addition, as the number of samples is increased from 360 to 1080, the MAE values of the TBNAM-ISFR reaches the minimum, which are 0.000681 Hz, 0.000260 Hz, and 0.000260 Hz, respectively, 0.000260Hz and 0.00346s.

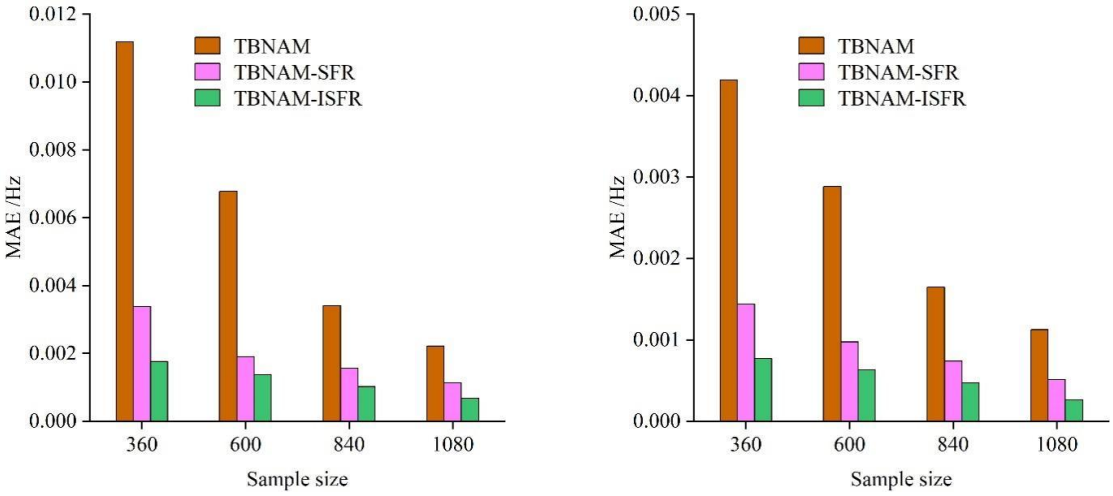

(a) Minimum frequency

(b) Steady-state frequency

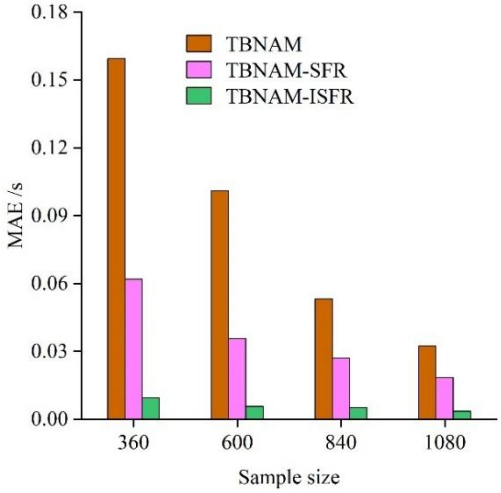

(c) Extreme value time

Figure 14: Prediction errors of each model under different sample sizes

(5) Impact of PMU installation ratio

In order to simulate the effect of insufficient PMUs on the predictive performance of the model, scenarios with different PMU installation ratios are set up in the IEEE14 node system. In each scenario, different buses are selected to be equipped with PMUs.The performance of the TBNAM-ISFR model with different PMU installation ratios is shown in Table 5.

As the number of PMUs in the system increases, the error level of the TBNAM-ISFR model decreases accordingly. This indicates that sufficient system measurement data will be favorable for the TBNAM-ISFR model to take advantage of its prediction. In addition, even if only the generator bus is equipped with PMUs, the error levels of TBNAM-ISFR are still within acceptable limits with MAEs of 0.000885 Hz, 0.000469 Hz, and 0.00402 s. This suggests that the TBNAM-ISFR model proposed in this paper is still able to reliably predict the frequency response characteristics in the case of insufficient PMUs.

Table 5: Prediction errors of ISFR-ALSTM models under different PMU installation ratios

Predicted object	Error index	The busbar with PMU installed		
		Only the generator busbar	Generator and load busbar.	All busbars
Minimum frequency	MAE /Hz	0.000885	0.000568	0.000492
	MAPE /%	0.819	0.531	0.447
	RMSE / Hz	0.00121	0.000739	0.000571
Steady-state frequency	MAE / Hz	0.000469	0.000281	0.000226
	MAPE /%	0.847	0.512	0.423
	RMSE / Hz	0.000632	0.000364	0.000291
Extreme value time	MAE /s	0.00402	0.00279	0.00205
	MAPE /%	0.134	0.0983	0.0716
	RMSE /s	0.00531	0.00358	0.00261

4.4.2 Actual system for the Fujian power grid

In order to analyze the effect of system size on the performance of the proposed model, the actual system of Fujian Power Grid was tested as a simulation system. Taking the 200 randomly selected samples in the minimum frequency prediction as an example, the prediction errors of

the ISFR model, the TBNAM model and the TBNAM-ISFR model are shown in Fig. 15. It can be seen that the ISFR model still ensures a certain prediction accuracy in a larger scale simulation system, which verifies the validity of the ISFR model in the real system. In addition, the prediction error of TBNAM-ISFR is overall smaller than that of the TBNAM model, proving the necessity of combining the ISFR model.

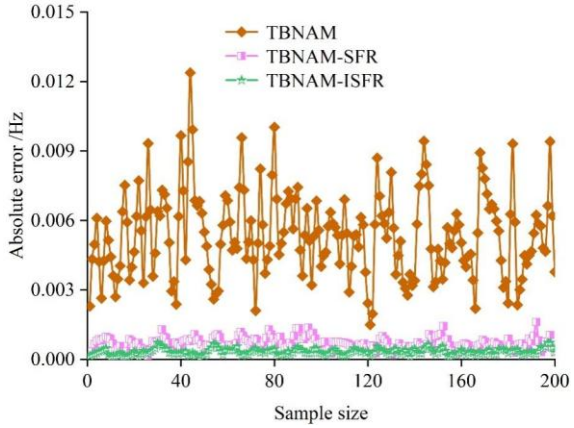

Figure 15: The absolute value of the lowest frequency prediction error in the actual system

In order to further demonstrate the superiority of the TBNAM-ISFR model in performance, the TBNAM-SFR model is introduced for a comprehensive comparison with the ELM- SFR fusion model. All the above models are tested with the same sample set, and the prediction results of MAE and MAPE metrics of each model in the real system are shown in Table 6.

Compared with the TBNAM model, the TBNAM-SFR model and the TBNAM-ISFR model show better performance with reduced MAE and MAPE metrics. Specifically, the MAE of the TBNAM-ISFR model is reduced to 0.000205 Hz, 0.000161 Hz, and 0.0883 s. Meanwhile, compared to the error metrics of the TBNAM-SFR model, the MAPE of the TBNAM-ISFR model is reduced by 0.422%, 0.333%, and 0.280%, respectively, proving that the combination of ISFR model is necessary and effective. As shown by the error metrics, the accuracy of the TBNAM-ISFR model is significantly better than that of the ELM-SFR model. On the one hand, the features provided by the ISFR model are more accurate than those provided by the traditional SFR model. On the other hand, unlike the ELM with a single hidden layer structure, the two-branch network integrating Bi-LSTM and CNN has a stronger feature learning capability, which can effectively utilize the system measurement data and more accurately fit the mapping relationship between the input features and the frequency response. In addition, the introduction of Attention mechanism can analyze the feature differences in different dimensions and assign appropriate weights to them, which further improves the model performance.

Table 6: The prediction results of each model in the actual system

Predicted object	Error index	Model			
		TBNAM	TBNAM-SFR	TBNAM-ISFR	ELM-SFR
Minimum frequency	MAE /Hz	0.000532	0.000438	0.000205	0.003289
	MAPE /%	0.914	0.761	0.339	4.693
Steady-state frequency	MAE / Hz	0.000411	0.000292	0.000161	0.002168
	MAPE /%	1.033	0.749	0.416	3.957
Extreme value time	MAE /s	0.1254	0.1160	0.0883	0.8594
	MAPE /%	1.185	1.096	0.816	9.319

Finally, the study shows that the training time of the TBNAM-ISFR model is 638.71 s, while the prediction time is only 0.21 ms. In summary, the TBNAM-ISFR model is able to satisfy both the accuracy and timeliness requirements in online applications.

5 Conclusion

In this paper, based on the data-physics fusion-driven power system digital twin framework, TBNAM-ISFR is constructed to realize the dynamic simulation of power system frequency response.

The proposed data-physics fusion dual-drive simulation algorithm, TBNAM-ISFR, is able to accurately obtain the results of each state variable and operation variable in the system, which is basically consistent with the PSAT reference results, and is suitable for the electromechanical transient simulation of power systems modeled by data-physics fusion drive. Moreover, the TBNAM-ISFR model achieves good simulation results for power system parameters under various scenarios such as step-length instability, step-length instability, step-length stability, step-length stability, etc., with the average absolute error of the power angle not exceeding 1.40%, and the average absolute error of the voltage magnitude not exceeding 0.22%, which indicates that the model has a good generalization ability to satisfy the computational needs of various scenarios.

Using the improved IEEE14 node system and the actual system of Fujian Power Grid for example analysis, the MAE, MAPE, and RMSE values predicted by the TBNAM-ISFR model at the minimum frequency, steady state frequency, and the pole time are all smaller than those of comparative models such as SFR, ISFR, TBNAM-SFR, and ELM-SFR, and they have a better prediction effect. Meanwhile, the training time of the TBNAM-ISFR model is 638.71s, while the prediction time is only 0.21ms, which can meet the real-time and accuracy requirements of the dynamic simulation of power systems.

This paper provides a new method for online frequency response analysis of power systems, which can improve the prediction accuracy while maintaining the prediction speed, but there is still much room for improvement due to the time limitation. The follow-up work can be carried out in the following aspects:

(1) The improved physical model proposed in this paper is only based on the current common generator model, which is insufficiently considered for the new energy generation model. Therefore, it is necessary to further improve the structure of the physical model to reserve modeling space for new energy devices that may be incorporated.

(2) The fusion model proposed in this paper only uses the serial fusion method for modeling, and the parallel, bootstrap, and feedback fusion methods have not been studied in depth. Therefore, these fusion methods can be utilized for further in-depth research.

Funding

This work was supported by State Grid Corporation of China Technology Project "Research and Application of Key Technologies for Digital Operation and Maintenance of Vacuum OLTC Based on Electromagnetic Transient Multidimensional Information Online Perception"（5500-202423167A-1-1-ZN）

About the Author

Pengfei Jia was born in Shanxi Province, China, in 1988. He obtained a master's degree from North China Electric Power University in China. I am currently studying at the School of Economics and Management, Wuhan University. He is currently is employed at the China Electric Power Research Institute, Co., Ltd., Beijing, China. His research interests include intelligent electrical appliances and electrical equipment. ABC20260312@163.com

Jiayun Zhu was born in Shanxi Province, China, in 1996. He received the B.E. degree from Taiyuan University of Technology, Shanxi, China, in 2018, and the M.S. degree from the School of Electrical Engineering, Xi'an Jiaotong University, Xi'an, China, in 2021, both in electrical engineering.

He is currently with the China Electric Power Research Institute, Co., Ltd., Beijing, China. His research interests include intelligent electrical appliances and electrical equipment. jyzhu0229@163.com

Huiyuan Zhang was born in Yantai, Shandong Province, P.R. China, in 1994. She obtained a Ph.D. degree from Beijing Jiaotong University in China. She is currently employed at the China Electric Power Research Institute, State Grid Corporation of China. Her main research direction is high voltage and insulation technology, flexible power transmission and transformation equipment, and equipment condition monitoring. zhanghyww@163.com

YuqiuLei was born in Baoji, Shaanxi, P.R. China, in 1991. She obtained a master's degree from Xi'an Jiaotong University in China. She is currently working at the China Electric Power Research Institute Co., Ltd. Her main research direction is high voltage technology. leiyuqiu@epri.sgcc.com.cn

References

[1] Matyushok, V., Vera Krasavina, V., Berezin, A., & Sendra Garcia, J. (2021). The global economy in technological transformation conditions: A review of modern trends. Economic Research-Ekonomska Istraživanja, 34(1), 1471-1497.

[2] Yang, L., & Liu, Q. (2021, August). A brief talk about the modern application of computer software technology and the development trend of research. In Journal of Physics: Conference Series (Vol. 1992, No. 4, p. 042024). IOP Publishing.

[3] Yao, J. F., Yang, Y., Wang, X. C., & Zhang, X. P. (2023). Systematic review of digital twin technology and applications. Visual computing for industry, biomedicine, and art, 6(1), 10.

[4] Botín-Sanabria, D. M., Mihaita, A. S., Peimbert-García, R. E., Ramírez-Moreno, M. A., Ramírez-Mendoza, R. A., & Lozoya-Santos, J. D. J. (2022). Digital twin technology challenges and applications: A comprehensive review. Remote Sensing, 14(6), 1335.

[5] Abo-Khalil, A. G. (2023). Digital twin real-time hybrid simulation platform for power system stability. Case Studies in Thermal Engineering, 49, 103237.

[6] Pan, H., Dou, Z., Cai, Y., Li, W., Lei, X., & Han, D. (2020, September). Digital twin and its application in power system. In 2020 5th international conference on power and renewable energy (ICPRE) (pp. 21-26). IEEE.

[7] Ruhe, S., Schaefer, K., Branz, S., Nicolai, S., Bretschneider, P., & Westermann, D. (2023). Design and implementation of a hierarchical digital twin for power systems using real-time simulation. Electronics, 12(12), 2747.

[8] Mohammadi Moghadam, H., Foroozan, H., Gheisarnejad, M., & Khooban, M. H. (2021). A survey on new trends of digital twin technology for power systems. Journal of Intelligent & Fuzzy Systems, 41(2), 3873-3893.

[9] Peyghami, S., Palensky, P., & Blaabjerg, F. (2020). An overview on the reliability of modern power electronic based power systems. IEEE Open Journal of Power Electronics, 1, 34-50.

[10] Jafari, M., Kavousi-Fard, A., Chen, T., & Karimi, M. (2023). A review on digital twin technology in smart grid, transportation system and smart city: Challenges and future. IEEe Access, 11, 17471-17484.

[11] Song, Z., Hackl, C. M., Anand, A., Thommessen, A., Petzschmann, J., Kamel, O., ... & Hauptmann, S. (2023). Digital twins for the future power system: An overview and a future perspective. Sustainability, 15(6), 5259.

[12] Palensky, P., Cvetkovic, M., Gusain, D., & Joseph, A. (2022). Digital twins and their use in future power systems. Digital Twin, 1, 4.

[13] Lei, Z., Zhou, H., Hu, W., Liu, G. P., & Guan, S. (2023). Web-based digital twin communication system of power systems for training and education. IEEE Transactions on Power Systems, 39(2), 3592-3602.

[14] Zhou, M., Yan, J., & Feng, D. (2019). Digital twin framework and its application to power grid online analysis. CSEE Journal of Power and Energy Systems, 5(3), 391-398.

[15] Kummerow, A., Nicolai, S., Brosinsky, C., Westermann, D., Naumann, A., & Richter, M. (2020, August). Digital-Twin based Services for advanced Monitoring and Control of future power systems. In 2020 IEEE Power & Energy Society General Meeting (PESGM) (pp. 1-5). IEEE.

[16] Arraño-Vargas, F., & Konstantinou, G. (2022). Modular design and real-time simulators toward power system digital twins implementation. IEEE Transactions on Industrial Informatics, 19(1), 52-61.

[17] Yassin, M. A., Shrestha, A., & Rabie, S. (2023). Digital twin in power system research and development: principle, scope, and challenges. Energy Reviews, 2(3), 100039.

[18] Khalyasmaa, A. I., Stepanova, A. I., Eroshenko, S. A., & Matrenin, P. V. (2023). Review of the digital twin technology applications for electrical equipment lifecycle management. Mathematics, 11(6), 1315.

[19] Li, Q., & He, Y. (2021). An overview of digital twin concept for key components of renewable energy systems. International Journal of Robotics and Automation Technology, 8, 29-47.

[20] Bai, H., & Wang, Y. (2022). Digital power grid based on digital twin: Definition, structure

and key technologies. Energy Reports, 8, 390-397.

[21] Chen, H., Zhang, Z., Karamanakos, P., & Rodriguez, J. (2022). Digital twin techniques for power electronics-based energy conversion systems: A survey of concepts, application scenarios, future challenges, and trends. IEEE Industrial Electronics Magazine, 17(2), 20-36.

[22] Cui, Y., Xiao, F., Wang, W., He, X., Zhang, C., & Zhang, Y. (2020, October). Digital twin for power system steady-state modelling, simulation, and analysis. In 2020 IEEE 4th Conference on Energy Internet and Energy System Integration (EI2) (pp. 1233-1238). IEEE.

[23] Ismail, F. B., Al-Faiz, H., Hasini, H., Al-Bazi, A., & Kazem, H. A. (2024). A comprehensive review of the dynamic applications of the digital twin technology across diverse energy sectors. Energy Strategy Reviews, 52, 101334.

[24] Wagner, T., Kittl, C., Jakob, J., Hiry, J., & Häger, U. (2024). Digital twins in power systems: a proposal for a definition. IEEE Power and Energy Magazine, 22(1), 16-23.

[25] Belik, M., & Rubanenko, O. (2023). Implementation of digital twin for increasing efficiency of renewable energy sources. Energies, 16(12), 4787.